Molecular Engineering of "Click"-Phospholes Towards Self-Assembled Luminescent Soft Materials

*Xiaoming He, Jian-Bin Lin, Wang Hay Kan, Pengcheng Dong, Simon Trudel, and Thomas Baumgartner**

Inspired by the self-assembled bilayer structures of natural amphiphilic phospholipids, a new class of highly luminescent "click"-phospholes with exocyclic alkynyl group at the phosphorus center is reported. These molecules can be easily functionalized with a self-assembly group to generate neutral "phosphole-lipids". This novel approach retains the versatile reactivity of the phosphorus center, allowing further engineering of the photophysical and self-assembly properties of the materials at a molecular level. The results of this study highlight the importance of being able to balance weak intermolecular interactions for controlling the self-assembly properties of soft materials. Only molecules with the appropriate set of intermolecular arrangement/interactions show both organogel and liquid crystal mesophases with well-ordered microstructures. Moreover, an efficient energy transfer of the luminescent materials is demonstrated and applied in the detection of organic solvent vapors.

1. Introduction

The self-assembly of luminescent materials with well-organized 1D or 2D structures has paramount importance for efficient energy- and charge-transport processes in the emerging field of organic electronics.[1,2] Among these soft materials, supramolecular organogels and liquid crystals are of particular interest because they can provide well-ordered bulk phases and are easily processable at low cost.[1,2] The specific organization into 1D- or 2D-supramolecular assemblies can be achieved through weak intermolecular interactions such as π–π stacking, hydrogen bonding, van der Waals forces, dipole-dipole and/or ionic interactions.[1,2] The optoelectronic properties of these soft materials, on the other hand, strongly rely on the π-conjugated central cores, which have mostly been based on neutral polycyclic aromatic hydrocarbons to date.[1,2]

The incorporation of inorganic main-group elements (e.g., B,[3] Si,[4] P[5]) into π-conjugated materials has recently created a promising new avenue for efficiently engineering the optoelectronic properties of conjugated materials at the molecular level by virtue of their unique structural (i.e., bonding) and electronic properties. Organophosphorus materials, in particular, offer great advantages over other main group species toward constructing self-assembled materials, due to the versatile reactivity of the P center (i.e., via modification of the lone pair with O, S, Me^+, BH_3 groups, or metal complexes).[5]

The groups of Weiss and Kato pioneered the study of phospholipid-like, self-assembled ionic phosphonium compounds, by focusing on systems with non-conjugated head groups.[6] Recently, we have combined the amphiphilic features of lipids with the valuable photophysical features of conjugated phospholes to generate several series of conjugated 'phosphole-lipid' and 'phosphinine-lipid' systems with π-conjugated head groups that led to self-assembled organogels and liquid crystal mesophases with intriguing photophysical and electrochemical behavior (**Scheme 1**a, top).[7] In this context, we were also able to unequivocally confirm the supramolecular bilayer organization of such lipid systems by X-ray crystallography.[7e] The strategy used for the molecular design of these first-generation conjugated organophosphorus-lipids, is the quaternization of the P center with an appropriate self-assembly moiety (Scheme 1a, top), which unfortunately blocks the P center from further functionalization and consequently precludes any further tuning of the optoelectronic properties via P-chemistry avenues.

Over the past several decades, there have been numerous efforts in incorporating a terminal alkynyl group into molecular systems as building block for the construction of molecular wires and optical materials, due to its linear geometry, structural rigidity, extended π-electron delocalization, and importantly, its diverse chemical reactivity.[8] Particularly, the Huisgen alkynyl–azide "click" reaction has gained considerable attention and has been widely used in the construction of organic conjugated materials because of its ease of synthesis, high functional group tolerance, and excellent reaction yields.[9] It is expected that incorporation of a terminal alkynyl group into a phosphole system would generate highly valuable functional materials. However, the very few examples reported by Matano and co-workers exclusively showcase α-alkynyl phosphole systems (Scheme 1b).[10]

Dr. X. M. He, Dr. J.-B. Lin, W. H. Kan, P. Dong, Prof. S. Trudel, Prof. T. Baumgartner
Department of Chemistry and Centre for Advanced Solar Materials
University of Calgary
2500 University Drive NW, Calgary, AB T2N 1N4, Canada
E-mail: thomas.baumgartner@ucalgary.ca

DOI: 10.1002/adfm.201302294

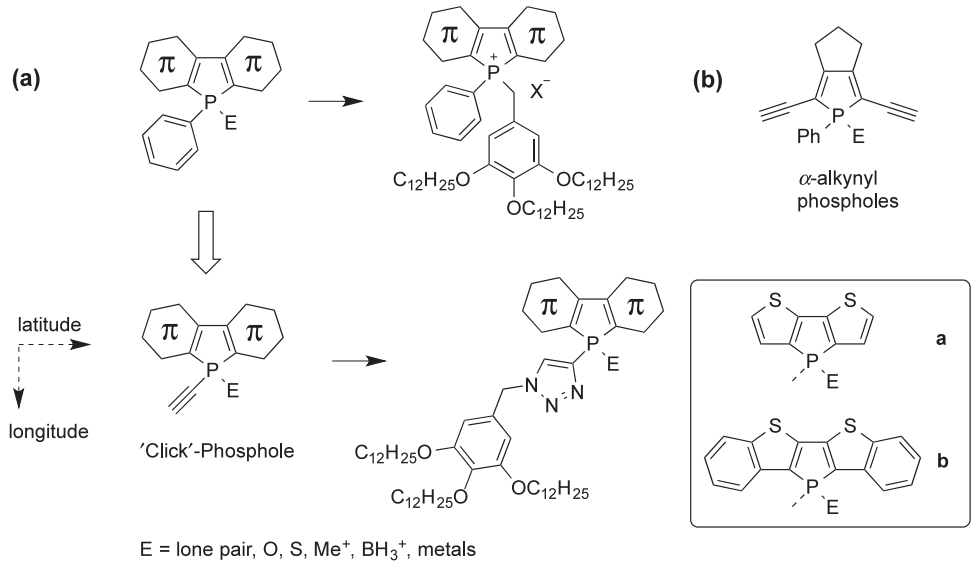

Scheme 1. (a) Top: original ionic 'phosphole-lipid' system; Bottom: current design strategy toward neutral phosphole-lipids using a "click"-phosphole; two conjugated heads (**a** and **b**) are used in this study. (b) Molecular structure of α-alkynyl phospholes reported by Matano et al.[10]

In this contribution, we now report a new class of longitudinally alkyne-functionalized phospholes (Scheme 1a, bottom). The installation of the alkynyl group at this position is expected to allow for further "click" reactions with appropriately functionalized azides, while the latitudinal direction along the building block is open for further tuning of the photophysical properties by incorporating aromatic moieties. Along these lines, two different π-conjugated head groups (**a**: dithienophosphole, **b**: bis(benzothieno)phosphole) have been chosen in order to influence potential π–π stacking interactions. Functionalization with self-assembly groups would then lead to a new class of neutral phosphole-lipids, where the phosphorus center is available for further engineering of the photophysical and self-assembly properties via P-modification (E). The "click"-functionalization of the new phospholes with azides affords an aromatic triazole substituent at the P-center that should be beneficial the overall stability of the scaffold, akin to the well-known, stable *P*-phenyl congeners.[11] Due to the sterically bulky nature of the pyramidal phosphorus center, it is not expected that this group would play a crucial role in the self-assembly behavior of the system. This paper now provides details on the synthesis, the photophysical and electrochemical properties, the molecular engineering toward self-assembly, as well as intriguing energy transfer and vapochromism of the new species.

2. Results and Discussion

2.1. Synthesis and Functionalization of the "Click"-Phospholes

The synthesis and functionalization of the new "click"-phospholes is shown in **Scheme 2**, and the detailed procedures are

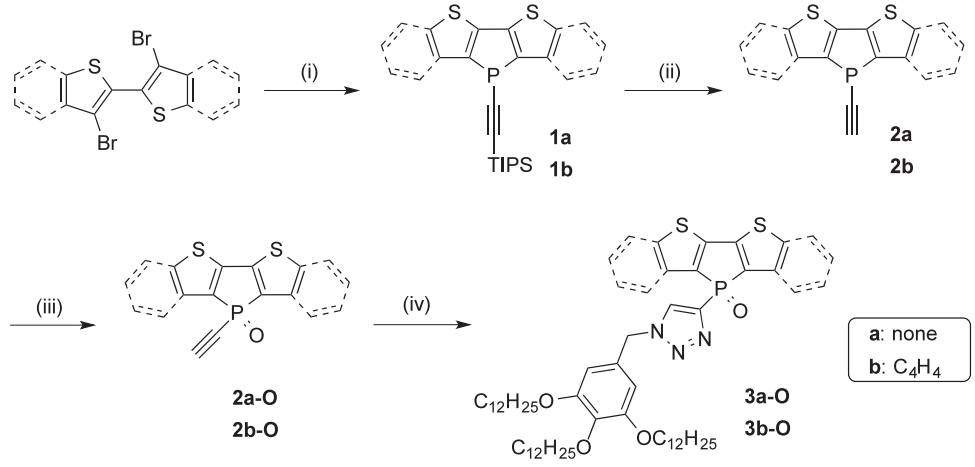

Scheme 2. Synthesis of "click"-phospholes and further functionalization with a self-assembly moiety. Reagents and conditions: i) *n*BuLi, Et_2O, –78 °C, 30 min, then $TIPSC{\equiv}CPCl_2$, Et_2O, rt, 2h; ii) TBAF, THF, –78 °C, 2h; iii) H_2O_2, THF/CH_2Cl_2 (1:1, v/v), rt, 2h; iv) CuI, DIPEA, THF, rt, 24h.

described in the Supporting Information. The central starting materials, the corresponding dibromoaryl precursors[11] and $TIPSC{\equiv}CPCl_2$[12] (TIPS = triisopropylsilyl) were prepared according to reported procedures. With the precursors in hand, two "click"-phospholes with different π-conjugated head groups, **1a** and **1b**, were synthesized in 45–60% yields according to our established procedures for *P*-phenyl phospholes[11] that involve the lithiation of the dibromo-precursors, followed by the addition of $TIPSC{\equiv}CPCl_2$ at low temperature. Deprotection of the TIPS group in compounds **1a** and **1b** was performed with tetrabutylammonium fluoride (TBAF) to afford **2a** and **2b** in 80–90% yield. The trivalent species (**2a**, **2b**) were then quantitatively oxidized with excess H_2O_2 to yield the respective phosphole oxides **2a-O** and **2b-O**.

In order to install self-assembly properties within the materials, the 3,4,5-tris(dodecyl-1-oxy)benzyl-group was successfully attached via Huisgen alkynyl-azide click reaction involving the corresponding azide, as well as the phosphole oxides **2a-O** and **2b-O**. The reaction proceeds under mild conditions by using CuI as catalyst and diisopropylethylamine (DIPEA) as base to generate the corresponding **3a-O** and **3b-O** in high yields (70–80%). It should be noted in this context that the click reactions using the trivalent species (**2a** and **2b**) were unsuccessful, probably due to the poisoning of CuI catalyst by coordination to the P center. All new compounds were fully characterized by ^1H, ^{13}C, and ^{31}P NMR spectroscopy, as well as high-resolution mass spectrometry. Moreover, the solid-state structure of **2b-O** was confirmed by X-ray crystallography; its discussion follows in a subsequent section.

The ^{31}P NMR-spectroscopic data for this family of phospholes are summarized in **Table 1**. The trivalent alkynyl phosphole systems (**1a**,**b**, **2a**,**b**) have ^{31}P NMR resonance signals in the range of -60 ± 4 ppm, which are highly upfield shifted compared to our previously reported trivalent dithienophosphole systems with *P*-phenyl group (c.f.: -20 ± 5 ppm).[11] Similar upfield-shifted ^{31}P NMR resonances were also observed with dithienophospholes that exhibit an electron-withdrawing pentafluorophenyl group at the P center (c.f.: −51.3 ppm),[11d] as well as somewhat related ferrocenylalkynylphosphanes that were reported by us in 2006.[13] The corresponding phosphole oxides also show similar upfield shifts in the ^{31}P NMR spectrum. When transforming the alkynyl moiety (**2a-O:** −10.9 ppm, **2b-O:** −12.0 ppm) into triazole (**3a-O:** +6.24 ppm, **3b-O:** +5.1 ppm), the ^{31}P NMR signals underwent a significant downfield shift by ca. +18 ppm, which was used as diagnostic tool for monitoring this reaction.

2.2. Modification of the P center

In order to further explore the availability of phosphorus chemistry avenues, the trivalent phosphole species (**3a** and **3b**) are necessary intermediates. The deoxygenation of the oxides **3a-O** and **3b-O** could be achieved in relatively high yield (90–92%) by reaction with trichlorosilane in refluxing toluene.[10b] With the trivalent species in hand, we could then further modify the phosphorus center to evaluate the effect on the self-assembly properties. Three typical modifications (gold-complex formation,

Table 1. ^{31}P NMR, photophysical, electrochemical and calculation data for the new phosphole compounds.

Compd	^{31}P NMR	Media	λ_{abs} [nm] (ε [$dm^3\ mol^{-1}\ cm^{-1}$])	λ_{em} [nm]	ϕ_{PL} [a]
1a	−56.0	CH_2Cl_2	289 (8260), 328 (8700)	429	0.24
2a	−59.6	CH_2Cl_2	282 (7800), 329 (9200)	423	0.35
2a-O	−10.9	CH_2Cl_2	372 (5730)	459	0.69
3a	−52.3	CH_2Cl_2	283 (9538), 331 (9500)	410	0.75
		Solid		449	
3a-O	+6.2	CH_2Cl_2	364 (5980)	452	0.55
		Gel		461	
		Solid		452	
3a-O-Me	−0.4	CH_2Cl_2	388 (5630)	490	0.33
3a-Au	−18.5	CH_2Cl_2	352 (5920)	433	0.71
1b	−59.0	CH_2Cl_2	339 (14820), 365 (14990)	435	0.48
2b	−63.1	CH_2Cl_2	338 (11610), 367 (13960)	438	0.57
2b-O	−12.0	CH_2Cl_2	336 (9210), 412 (7960)	505	0.82
3b	−52.2	CH_2Cl_2	340 (18920), 368 (22120)	434	0.35
		Solid		482	
3b-O	+5.1	CH_2Cl_2	333 (9160), 403 (9710)	498	0.58
		Gel		512	
		Solid		523	
3b-O-Me	−2.1	CH_2Cl_2	346 (14370), 431 (9200)	535	0.35

[a] Fluorescence quantum yield, relative to quinine sulfate (0.1 M H_2SO_4 solution); excitation at 365 nm.

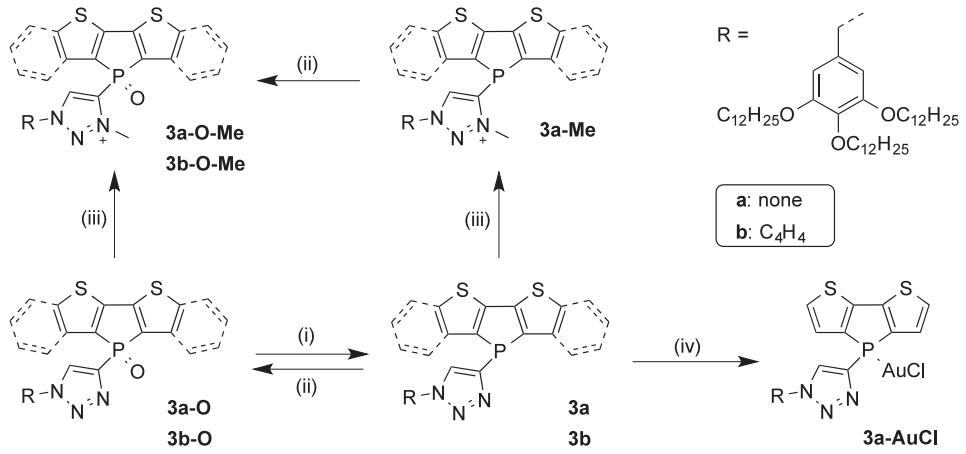

Scheme 3. A family of new phosphole compounds through *P*-modification. Reagents and conditions: i) $HSiCl_3$, toluene, 110 °C, 2h; ii) H_2O_2, THF, rt, 2h; iii) MeOTf, CH_2Cl_2, rt, 12h; iv) Au(tht)Cl, CH_2Cl_2, rt, 2h.

methylation, oxidation) were carried out to elaborate the potential reactivity of the trivalent phosphorus center (**Scheme 3**).

The conversion to the gold complex **3a-AuCl** was readily achieved by reaction of **3a** with Au(tht)Cl (tht = tetrahydrothiophene) in CH_2Cl_2 at room temperature. Moreover, previous work by others and our group has revealed that ionic interactions of cationic phosphonium salts can provide the necessary driving force for the formation of soft materials, such as liquid crystals and organogels.[6,7] To this end, trivalent species **3a** and **3b** were reacted with methyl triflate (MeOTf) in order to quaternize the P center. However, *N*-methylation of the triazole unit was observed exclusively (Scheme 3), even in the presence of a large excess of MeOTf (10 eq.), which indicates a much higher Lewis basicity of nitrogen over that of phosphorus. Similar results were also observed for trivalent azadibenzophosphole systems.[14] The methylation also occurs at the same nitrogen position with the phosphole oxide species **3a-O** and **3b-O**. The reactivity of **3a** and **3a-O** towards MeOTf was investigated in greater detail by titration experiments and monitored via ^{31}P NMR spectroscopy (Figure S1 and S2). After methylation, the ^{31}P NMR signals for both the trivalent and the phosphole oxide species underwent an upfield shift by ca. 7–14 ppm (Table 1), which could be attributed to electronic effects.[11d] In addition, the reactivity of the trivalent **3a** is much higher than that of **3a-O**, in line with the reduced Lewis basicity of the N-atom in **3a-O** due to the increased electron-accepting features of the P=O moiety vs. a trivalent P-center. On the other hand, the oxidation of the trivalent species **3a-Me** could be achieved easily by reaction with H_2O_2. Overall, as shown in Scheme 3, a family of new phosphole derivatives can be prepared, allowing us to further investigate the potential tuning of their photophysical, electrochemical, as well as self-assembly properties.

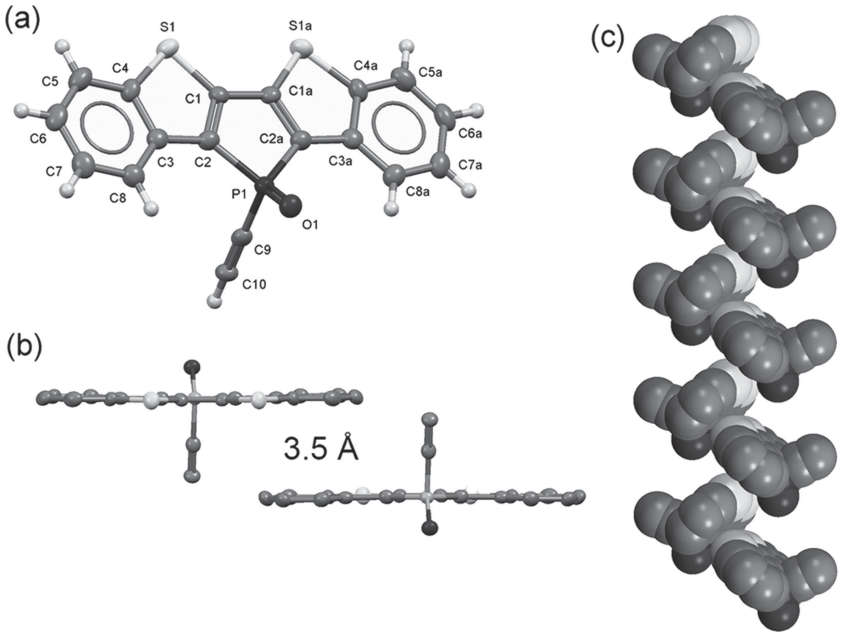

Figure 1. (a) Molecular structure of **2b-O** in the solid state (50% probability level), Selected bond lengths [Å] and angles [°]: P1-O1 1.483(6), P1-C2 1.785(6), P1-C9 1.749(9), C1-C2 1.370(8), C1-C1a 1.441(9), S1-C1 1.718(6), S1-C4 1.749(6), O1-P1-C2 118.8(3), O1-P1-C9 113.4(4); (b) Molecular packing of **2b-O**; (c) Space-filling representation of the edge-to-face herringbone-type arrangement with weak O···S interactions between neighboring molecules in the structure of **2b-O** (H atoms omitted for clarity).

2.3. Solid-State Structure

The molecular arrangement and packing in the solid state play an important role for the generation of self-assembled materials. Single crystals of compound **2b-O** that were suitable for X-ray crystallography were obtained from the slow evaporation of a concentrated CH_2Cl_2 solution. The molecular structure and solid-state packing of **2b-O** are shown in **Figure 1**. The crystal data and structure refinement are summarized in Table S1 in the Supporting Information. The

single molecule is highly symmetrical and all bond lengths and angles are comparable to those observed for previously reported *P*-phenyl heteropentacene dithienophospholes.[11c] In terms of molecular packing, intermolecular π–π interactions between neighboring conjugated backbones (at about 3.5 Å) are observed. In addition, the molecules are organized in a highly ordered one-dimensional edge-to-face herringbone-type arrangement, similar to that observed for many other pentacene derivatives.[15] Remarkably, similar to the *P*-phenyl congener,[11c] a peculiar O···S interaction is observed for **2b-O** between the P=O group with the two thiophene S-atoms of a neighboring molecule. However, the distance of (3.84 Å) in the current case is larger than in the previously reported *P*-phenyl dithienophosphole heteropentacene (c.f. 2.80 Å), probably due to electronic effects from the different exocyclic substituents at the phosphorus center.

Notably, such kind of herringbone organization is not observed for either the regular dithienophospholes, or other related pentacene phosphole derivatives with different *P*-modification (P=S and P-Me$^+$). The heteropentacene phosphole oxide species thus show a solid-state packing that is unique for the whole family, and it also strongly impacts the self-assembly properties of **3b-O** (vide infra).

2.4. Photophysical and Electrochemical Properties

The photophysical data of the highly fluorescent new phosphole compounds are summarized in Table 1. Compared to the *P*-phenyl substituted dithienophosphole oxide (λ_{abs} = 361 nm, λ_{em} = 446 nm)[11a] and heteropentacene dithienophosphole oxide (λ_{abs} = 385 nm, λ_{em} = 483 nm),[11c] both the absorption and emission maxima of corresponding "click"-phospholes **2a-O** (λ_{abs} = 372 nm, λ_{em} = 459 nm) and **2b-O** (λ_{abs} = 403 nm, λ_{em} = 505 nm) show a modest red shift. After transformation of the alkynyl moieties to the triazole species, slightly blue-shifted absorption and emission were observed for **3a-O** (λ_{abs} = 364 nm, λ_{em} = 452 nm) and **3b-O** (λ_{abs} = 403 nm, λ_{em} = 498 nm). Gold complex **3a-AuCl** (λ_{abs} = 352 nm, λ_{em} = 433 nm) shows blue-shifted optical features compared with that of **3a-O** and no transitions resulting from aurophilic interactions are observed.

The emission properties of the **3** series were further investigated in detail by comparing the CH_2Cl_2 solution data with those in the solid state, in order to get some deeper insight into the molecular organization of the species in the different states. As shown in **Figure 2**, the emission of all compounds shows a large red shift in the solid state. According to our previous studies, this observation can be ascribed to the presence of π–π interaction in the solid state.[7d]

The trivalent species **3a** ($\Delta\lambda_{em}$ = 39 nm) and **3b** ($\Delta\lambda_{em}$ = 38 nm) show larger red-shifted emissions in the solid state than the corresponding phosphole oxides **3a-O** ($\Delta\lambda_{em}$ = 0 nm) and **3b-O** ($\Delta\lambda_{em}$ = 25 nm), indicating an efficient intermolecular π–π interaction for the trivalent species, whereas the data for **3a-O** (with small conjugated core) suggest the absence of such interactions. Overall, these data provide valuable information for the molecular packing in the solid state, which will be further discussed in the next section.

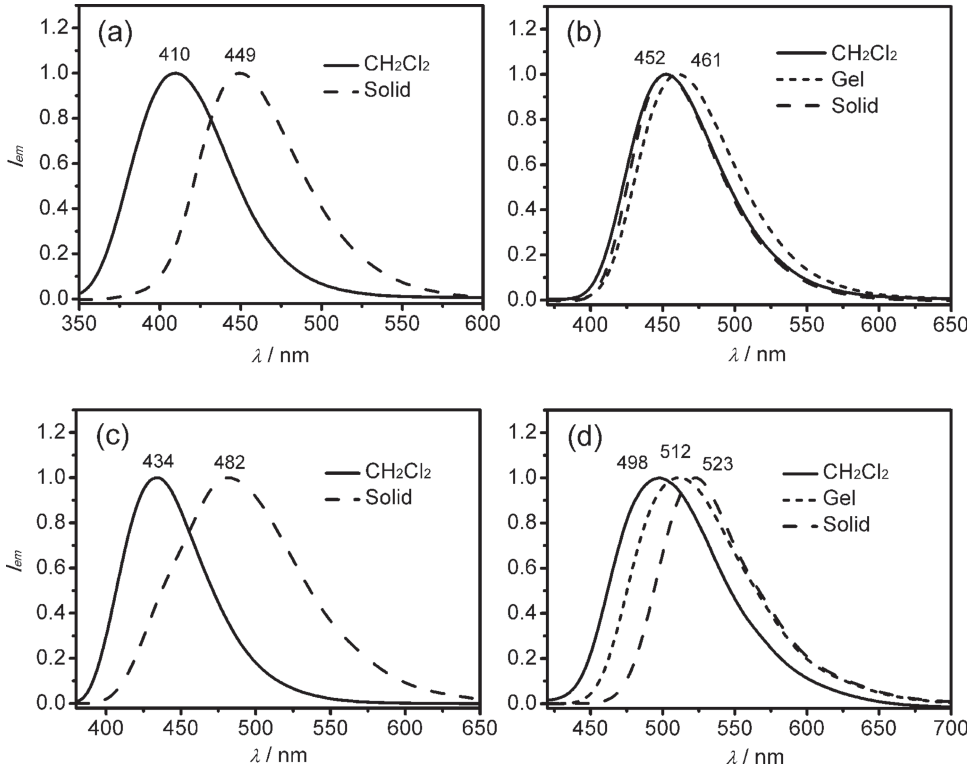

Figure 2. Emission spectra of **3a** (a), **3a-O** (b), **3b** (c) and **3b-O** (d) in different states (CH_2Cl_2, solid, and gel).

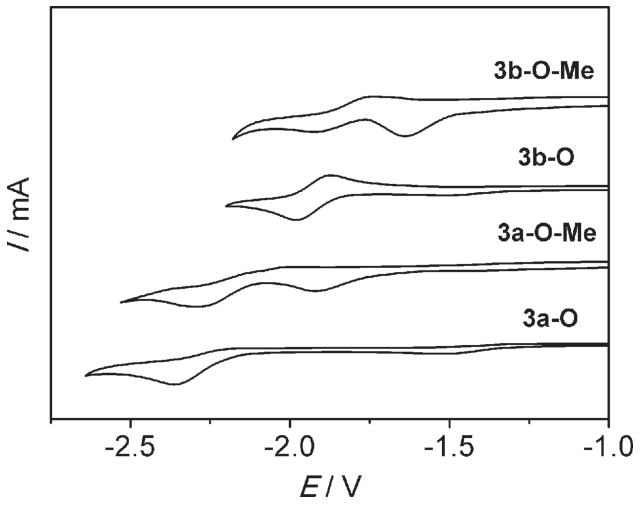

Figure 3. Cyclic voltammograms of compounds **3a-O**, **3a-O-Me**, **3b-O** and **3b-O-Me** in CH_2Cl_2 with 0.1M tetrabutylammonium hexafluorophosphate as a supporting electrolyte. Scan rate: 100 mVs^{-1}. Ferrocene was added as internal standard and referenced to 0 V.

N-methylation of **3a-O** ($\Delta\lambda_{abs}$ = 24 nm, $\Delta\lambda_{em}$ = 37 nm) and **3b-O** ($\Delta\lambda_{abs}$ = 28, $\Delta\lambda_{em}$ = 37 nm) leads to further red-shifted UV-vis absorption and emission values (Table 1 and Figure S4). In particular, the fluorescence of **3a-O** and **3b-O** in CH_2Cl_2 solution visibly changes from blue to green (for **3a-O-Me**), and from green to yellow (for **3b-O-Me**), respectively. This feature can be attributed to the generation of a stronger electron-accepting moiety upon methylation; a similar red-shifted fluorescence emission was observed for the dithienophosphole system upon introducing a electron-withdrawing pentafluorophenyl group at phosphorus ($\Delta\lambda_{em}$ = 56 nm).[11d] To further demonstrate the increased electron-accepting properties, the electrochemical properties of **3a-O** and **3b-O**, as well as two methylated compounds (**3a-O-Me** and **3b-O-Me**) were investigated by cyclic voltammetry (vs. ferrocene/ferrocenium; **Figure 3**). Indeed, the methylated compounds **3a-O-Me** (E_{red} = −1.85, −2.15 V) and **3b-O-Me** (E_{red} = −1.58, −1.84 V) show lower reduction potentials than their corresponding non-methylated congeners **3a-O** (E_{red} = −2.17 V) and **3b-O** (E_{red} = −1.92 V), indicating a considerable increase in the electron-accepting ability upon methylation. In contrast to the non-methylated species that only have one reduction peak, the methylated species exhibit two reduction processes, probably due to their cationic nature that can help counterbalance the negative charge formed during the process.[7e] However, among these four compounds, only **3b-O** shows a fully reversible reduction process.

2.5. Self Assembly (Organogel)

Organogels are interesting soft materials that can entrap large volumes of solvents in self-assembled networks through various balanced weak intermolecular interactions. Moreover, organogelators based on functional chromophores and dyes have also attracted significant interest as novel functional materials for a variety of optoelectronic applications in recent years.[1] Most of the research to date has focused on the combination of various chromophores with self-assembly units,[1] however, much less efforts have been invested in tuning the intermolecular weak interactions to control the self-assembly behavior by simple molecular modifications. The family of new compounds reported herein thus provides a great opportunity towards addressing this feature via molecular engineering of the conjugated head groups, modification of the P-center, as well as the introduction of an ionic charge at the N-atom. Interestingly, only the two neutral phosphole oxides **3a-O** and **3b-O** form organogels in hydrocarbon solvents (i.e., hexane and heptane). Gel formation requires the heating of the heterogeneous solvent/gelator mixture to access a homogeneous clear solution phase that upon cooling to room temperature in air forms an organogel. The critical gel concentration (CGC) for **3b-O** (ca. 4.0 mg mL^{-1}) with large π-conjugated core was determined to be much smaller than that of **3a-O** (ca. 8.5 mg mL^{-1}) with small core, conceivably resulting from its potential for stronger π–π interaction from the larger aromatic core. In stark contrast to the opaque organogel of **3a-O**, **3b-O** forms a fully transparent gel, which suggests a highly organized structure in the gel state of the latter. In addition, the gel formation process of **3b-O** (ca. 0.5 hour) is much faster than **3a-O** (ca. 2 hours), indicating a slower molecular reorganization and weaker intermolecular interactions for **3a-O** in the gel state. Both organogels of **3a-O** and **3b-O** exhibited thermally reversible sol-to-gel phase transitions and the thermal stability of the two species (as solids) was evaluated by thermogravimetric analysis (TGA) (Figure S5). The decomposition temperatures (defined as the temperatures of 5% mass loss) were determined to lie over 300 °C, indicating high thermal stability.

When exposed UV irradiation (365 nm), the organogels of **3a-O** and **3b-O** exhibit strong blue and green luminescence, respectively (**Figure 4**a and b); the emission spectra are shown in Figure 2. For **3b-O**, the emission maximum of the gel (λ_{em} = 512 nm) lies in between that of the solution (λ_{em} = 498 nm) and the solid state (λ_{em} = 523 nm), indicating somewhat weakened intermolecular interactions in the gel, conceivably due to the presence of the solvent. By contrast, the emission maximum of **3a-O** in the gel state exhibits a red shift (λ_{em} = 461 nm) compared to the solid state.

To further elucidate the self-assembly process and morphology of the materials, scanning electron microscopy (SEM) was performed on the dried gels of **3a-O** and **3b-O**, which were prepared by placing a slice of the freshly prepared gel onto a carbon-tape coated standard aluminum stub. In fact, the micromorphology of the gels is strongly dependent on the π-conjugated cores. Interestingly, as shown in Figures 4c and d, **3b-O** forms a very thin and smooth film on the surface with some rod-like wrinkles. A closer look reveals that both the smooth film and wrinkles are actually composed of a series of highly regular 1D self-assembled fibers with an average diameter of about 70 nm. The presence of 1D nanofibers in the organogel of **3b-O** from hexane was further confirmed by confocal fluorescence microscopy (Figure S6). Notably, this morphology was not observed for **3a-O**, whose xerogel rather forms a 3D network of microscopically entangled 1D fibers (Figure S7). This observation clearly illustrates the crucial effects of the different π-conjugated scaffolds on the self-assembly behavior of these two materials.

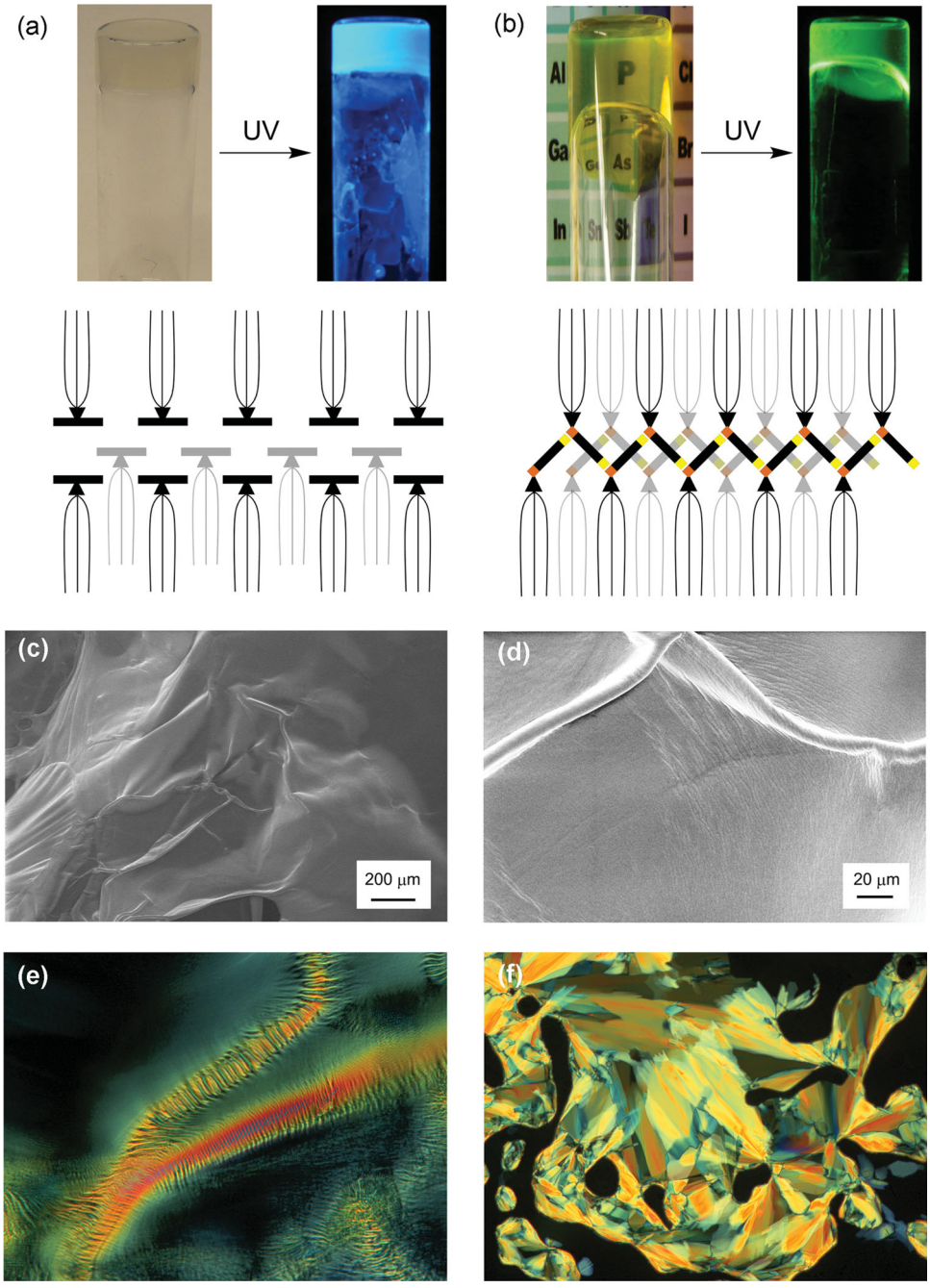

Figure 4. (a) Top: Opaque organogel of **3a-O** in hexane before (left) and after (right) UV irradiation; Bottom: Proposed molecular organization for **3a-O** in the self-assembled gel phase. (b) Top: Transparent organogel of **3b-O** before (left) and after (right) UV irradiation; Bottom: Proposed molecular organization for **3b-O** in the self-assembled gel phase. (c) and (d) Variable-pressure SEM images of a xerogel of **3b-O** obtained from hexane (landing energy = 20 kV, ambient pressure = 30 Pa). (e) Polarized optical micrograph of the xerogel of **3b-O** at room temperature. (f) Polarized optical micrograph of neat **3b-O** at 110 °C.

The proposed molecular organizations for the organogels of **3a-O** and **3b-O** are shown in Figures 4a and b. Based on the solid-state packing of **3b-O** determined by X-ray crystallography, it is inherently plausible to propose that the well-organized film results from multiple synergetic driving forces, such as O···S interactions, π–π stacking and intermolecular hydrophobic interactions between the long alkoxy chains; the O···S interactions in the gel state of **3b-O** is also supported by IR spectroscopy (Figure S9). However, **3a-O** with small π-conjugated core only has the latter two driving forces, highlighting the benefits of the weak O···S interactions in the formation of self-assembled soft materials that has never been noticed before.

As mentioned above, gel formation was not observed for the trivalent species in this family (**3a** and **3b**), further indirectly

validating the importance of the O···S interaction. In addition, the trivalent species likely do have stronger π–π interactions than their *P*-oxo counterparts. All of the results highlight the crucial importance of correctly balancing the delicate intermolecular interactions for the formation of soft materials. Interestingly, when the concentrated hexane solution of **3b** was exposed to air (i.e., O_2), a partial gel with strong green emission was formed, as the result of the oxidation of **3b** to **3b-O**. This "off–on" gel formation consequently may offer a promising approach to detect oxygen.

We were also interested in investigating the effect of ionic interactions on the self-assembly behavior of the new materials via **3a-O-Me** and **3b-O-Me**. However, these two compounds were found to also not form organogels, suggesting that intermolecular ionic interactions are in fact a counterproductive feature for creating self-assembled organogels with these species.

2.6. Self Assembly (Liquid Crystals)

As mentioned in the introduction, another intriguing form of self-assembled functional materials are liquid crystals.[2] After screening this family of new phospholes for this property, only compound **3b-O** showed liquid crystalline behavior. The liquid crystal properties of **3b-O** were investigated by differential scanning calorimetry (DSC), polarized optical microscopy (POM) and variable-temperature powder X-ray diffraction (VT-PXRD). The DSC experiments revealed several thermal phase transitions (**Figure 5**a). Upon heating **3b-O** from −50 °C, one endothermic (at 103 °C) and one exothermic (at 110 °C) transition were observed, which were tentatively assigned to a solid-to-liquid crystal, and liquid crystal-to-liquid crystal transition, respectively. As the temperature increased to 143 °C, compound **3b-O** started to exhibit phase transitions to an isotropic liquid, where a dark homeotropic area was observed. The return cooling showed two exothermic signals at 121 °C (small) and 74 °C (intense), which were assigned to the liquid-to-liquid crystal, and liquid crystal-to-soft crystal transitions. Multiple DSC scans revealed reversibility, supporting high stability of the compound. The formation of a liquid crystal phase of **3b-O** was also confirmed by POM (Figure 4f). Surprisingly, the dried gel sample moreover showed liquid (or soft) crystal properties at room temperature, and the POM texture indicated a highly organized 1D-fiber assembly, consistent with the observation from SEM and confocal fluorescence microscopy (Figure 4e), which could generally provide for an easy processing of liquid crystal materials from self-assembled gels.

The liquid crystalline nature and phase transitions of **3b-O** were further supported by VT-PXRD experiments (Figure 5b). The sample was first melted at its isotropic liquid phase state (150 °C), where no signals were observed, suggesting an amorphous phase as would be expected for melts. Upon cooling to 110 °C, a single sharp peak appeared at $2\theta = 2.2$, corresponding to a *d*-spacing value of 40.1 Å, which was assigned to a smectic phase indexed to the (100) plane, according to our previous studies.[7] However, the thickness of the layer (*d*-spacing) of **3b-O** is much larger than our previously reported phospholelipid or phosphinine-lipid system ($d \approx 26$–27 Å),[7] suggesting weaker van der Waals interactions in current system. On the other hand, a similarly clear phase transition was not observed for **3a-O** in the VT-PXRD experiments (Figure S10).

2.7. Energy Transfer and Vapochromism

Luminescent organogels provide a high degree of self-organization for luminophores, which has been recognized as crucial for efficient energy-transfer species that mimic natural light-harvesting systems.[1a,16] Given the broad spectral overlap between the fluorescence of **3b-O** (as donor) and the absorption of Rhodamine B (as acceptor) (Figure S11), it was expected that efficient fluorescence resonance energy transfer (FRET) would occur in a mixture of the two species.[1a,7b,16] Because of the low solubility of Rhodamine B in the hydrocarbon solvents used for the gelation, the energy-transfer process was studied in the solid state instead of the gel state.[17] **Figure 6**a shows the emission spectral changes of a drop-cast film of **3b-O** (from CH_2Cl_2 solution) blended with 1 mol% of Rhodamine B. Remarkably, the energy-transfer process was found to heavily rely on the presence of solvent residues. Upon prolonged evaporation times, the emission from Rhodamine B gradually increased, while the emission of **3b-O** concomitantly decreased.

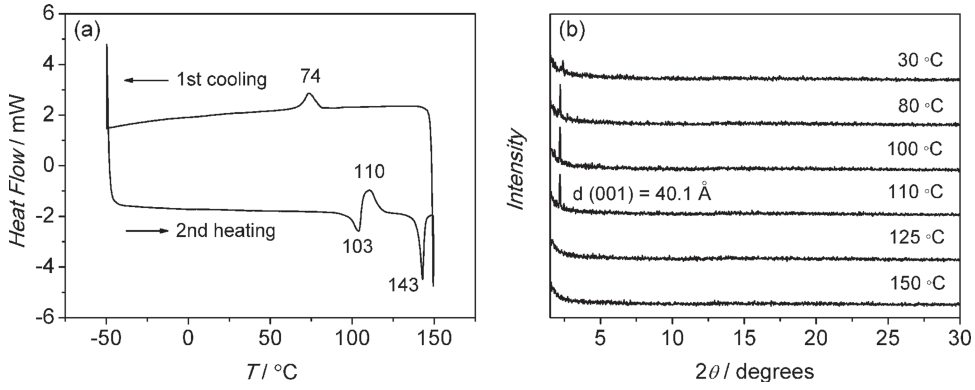

Figure 5. (a) DSC traces of **3b-O** with the heating and cooling rate at 5 °C min^{-1} (negative heat flow values indicate an endothermic process); (b) powder X-ray diffraction of **3b-O** at variable temperatures.

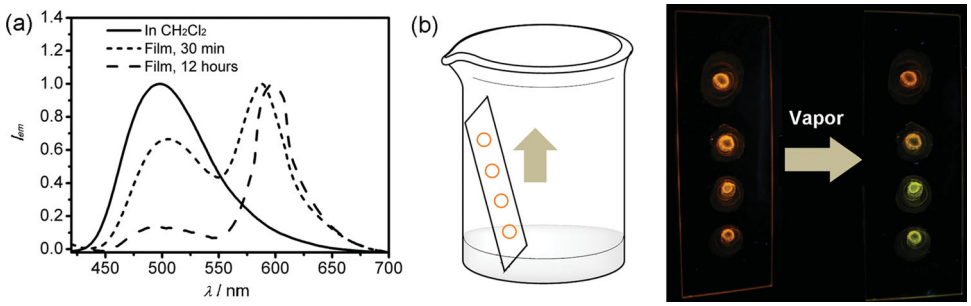

Figure 6. a) Emission spectra of **3b-O**:Rhodamine B (100:1) mixture in CH_2Cl_2 solution (solid line) and the solid state (dotted, dashed lines). b) Picture showing the experimental setting (left) and fluorescent vapochromism (right).

Complete energy transfer was found to occur after ca. 12 h. Such sensitivity towards trace of solvent residue is quite useful and could be utilized in the detection of volatile organic compound (VOC) vapors.[18] Indeed, as shown in Figure 6b, four spots composed of **3b-O**:Rhodamine B (100:1) film were prepared by drop-casting and dried overnight for efficient energy transfer to occur.

When exposed to various solvent vapors (CH_2Cl_2, $CHCl_3$, diethyl ether, acetone and methanol), the lower spots change their emission color very quickly from orange to green, while the top spots without exposure to vapor keep their original orange emission color. Despite the lack of selectivity, this process could find potential utility in general air quality testing indicating the presence of VOCs.

3. Conclusion

In conclusion, the synthesis of a family of novel "click"-phospholes and their molecular engineering toward highly luminescent phosphole-lipid soft materials is reported. The photophysical, electrochemical, and particularly self-assembly properties can be tuned by tailoring the π-conjugated phosphole heads, as well as simple modifications of the P- and N-centers. Among this family, compound **3b-O** shows the best self-assembly behavior leading to highly ordered structures in the presence, but also absence of solvents. The self-assembled microstructures were investigated with SEM, VT-PXRD, confocal fluorescence microscopy and POM. These results suggest that **3b-O** has the most balanced intermolecular interactions (π–π stacking, O···S interaction, hydrophobic–hydrophobic interactions) that lead to a suitable molecular arrangement for the formation of both organogels and liquid crystals. A practical application of the intriguing self-assembly and luminescent properties of **3b-O** involves the energy transfer studies between **3b-O** and Rhodamine B in a thin film. The energy transfer is found to be strongly dependent on the presence of solvent residues, and can successfully be applied in organic solvent vapor detection.

4. Experimental Section

Materials and Synthesis: All chemical reagents were purchased from commercial sources (Sigma-Aldrich, Alfa Aesar, Strem) and were, unless otherwise noted, used without further purification. Solvents were dried using an MBraun solvent purification system prior to use. Dibromo-precursors[11] and TIPSC≡CPCl$_2$[12] were prepared according to reported procedures. The detailed synthetic procedures and characterization for the new compounds are described in the Supporting Information. All reactions and manipulations were carried out under a dry nitrogen atmosphere employing standard Schlenk techniques.

Instruments and Methods: $^{31}P\{^1H\}$ NMR, ^1H NMR, and $^{13}C\{^1H\}$ NMR were recorded on Bruker DRX400 and Avance (-II,-III) 400 MHz spectrometers. Chemical shifts were referenced to external 85% H_3PO_4 (^{31}P) or residual non-deuterated solvent peaks (^1H, ^{13}C). Elemental analyses were performed in the Department of Chemistry at the University of Calgary. Mass spectra were run on a Finnigan SSQ 7000 spectrometer or a Bruker Daltonics AutoFlex III system. All photophysical experiments were carried out on a Jasco FP-6600 spectrofluorometer and UV/vis–NIR Cary 5000 spectrophotometer. Cyclic voltammetry analyses were performed on an Autolab PGSTAT302 instrument, with a polished glassy carbon electrode as the working electrode, a Pt-wire as counter electrode, and an Ag/AgCl/KCl 3M reference electrode, using ferrocene/ferrocenium as internal standard. If not otherwise noted, cyclic voltammetry experiments were performed in dichloromethane solution with tetrabutylammonium hexafluorophosphate (0.1 M) as supporting electrolyte. Crystal data and details of the data collection are provided in Table S1. Diffraction data were collected on a Nonius Kappa CCD diffractometer, using Mo Kα radiation (λ) 0.71073 Å (graphite monochromator). The structures were solved by direct methods (SHELXTL) and refined on F^2 by full-matrix least-squares techniques. CCDC-949092 contains the supplementary crystallographic data of 2b-O for this paper. These data can be obtained free of charge from The Cambridge Crystallographic Data Centre via www.ccdc.cam.ac.uk/data_request/cif. Scanning electron microscopy was performed using a Zeiss Σigma VP microscope equipped with a field-emission gun. Xerogels of **3a-O** and **3b-O** in hexane were prepared by placing a slice of the freshly prepared gel onto a carbon-tape coated standard aluminum stub, and imaging the samples as rapidly as possible following loading into the instrument chamber. For all samples secondary electron images were acquired with a landing energy of 20 kV in variable pressure mode (P = 29 to 30 Pa of air) to mitigate the effects of charging. Fluorescence confocal microscopy was performed on Leica inverted confocal TCS SP2 with water immersion lense. Powder XRD was measured by using Bruker Advance D8 powder X-ray diffractometer (CuKα, 40 kV, 40 mA). Thermal analyses were performed using TA-Q200 DSC instrument.

Preparation of Materials for Vapor Detection: A CH_2Cl_2 solution containing **3b-O** (1 mM) and Rhodamine B (1.0×10^{-5} M) was prepared, followed by deposition of the solution to 4 spots on a glass slide by drop casting. Then the glass slide was air-dried overnight before the experiment.

Supporting Information

Supporting Information is available from the Wiley Online Library or from the author.

Acknowledgements

Financial support by the NSERC of Canada, as well as the Canada Foundation for Innovation (CFI) is gratefully acknowledged. We thank Prof. T. Sutherland for the generous use of his UV/Vis spectrometer and electrochemistry equipment. We are grateful to C. Stremick and A. Y. Y. Woo for the kind help with fluorescent confocal microscopy and IR spectroscopy, respectively.

Received: July 8, 2013
Published online: August 8, 2013

[1] a) A. Ajayaghosh, V. K. Praveen, C. Vijayakumar, *Chem. Soc. Rev.* **2008**, *37*, 109; b) X. Yang, G. Zhang, D. Zhang, *J. Mater. Chem.* **2012**, *22*, 38; c) J. W. Steed, *Chem. Commun.* **2011**, *47*, 1379; S. Diring, F. Camerel, B. Donnio, T. Dintzer, S. Toffanin, R. Capelli, M. Muccini, R. Ziessel, *J. Am. Chem. Soc.* **2009**, *131*, 18177.

[2] a) L. Schmidt-Mende, A. Fechtenkötter, K. Müllen, E. Moons, R. H. Friend, J. D. MacKenzie, *Science* **2001**, *293*, 1119; b) E. J. Foster, R. B. Jones, C. Lavigueur, V. E. Williams, *J. Am. Chem. Soc.* **2006**, *128*, 8569; c) A. Wicklein, A. Lang, M. Muth, M. Thelakkat, *J. Am. Chem. Soc.* **2009**, *131*, 14442; d) Z. An, J. Yu, S. C. Jones, S. Barlow, S. Yoo, B. Domercq, P. Prins, L. D. A. Siebbeles, B. Kippelen, S. R. Marder, *Adv. Mater.* **2005**, *17*, 2580; e) Z. Chen, U. Baumeister, C. Tschierske, F. Würthner, *Chem. Eur. J.* **2007**, *13*, 450; f) A. D. Bromby, W. H. Kan, T. C. Sutherland, *J. Mater. Chem.* **2012**, *22*, 20611.

[3] a) F. Jäkle, *Chem. Rev.* **2010**, *110*, 3985; b) C. R. Wade, A. E. J. Broomsgrove, S. Aldridge, F. P. Gabbaï, *Chem. Rev.* **2010**, *110*, 3958; c) Z. M. Hudson, S. Wang, *Acc. Chem. Res.* **2009**, *42*, 1584; d) L. G. Mercier, W. E. Piers, M. Parvez, *Angew. Chem.* **2009**, *121*, 6224; *Angew. Chem. Int. Ed.* **2009**, *48*, 6108; e) A. Wakamiya, K. Mori, S. Yamaguchi, *Angew. Chem.* **2007**, *119*, 4351; *Angew. Chem. Int. Ed.* **2007**, *46*, 4273; f) M. Elbing, G. C. Bazan, *Angew. Chem.* **2008**, *120*, 846; *Angew. Chem. Int. Ed.* **2008**, *47*, 834; g) S. Saito, K. Matsuo, S. Yamaguchi, *J. Am. Chem. Soc.* **2012**, *134*, 9130; h) Z. Zhou, A. Wakamiya, T. Kushida, S. Yamaguchi, *J. Am. Chem. Soc.* **2012**, *134*, 4529.

[4] a) S. Yamaguchi, K. Tamao, *J. Chem. Soc., Dalton Trans.* **1998**, 3693; b) J. Chen, Y. Cao, *Macromol. Rapid Commun.* **2007**, *28*, 1714; c) T.-Y. Chu, J. Lu, S. Beaupré, Y. Zhang, J.-R. Pouliot, S. Wakim, J. Zhou, M. Leclerc, Z. Li, J. Ding, Y. Tao, *J. Am. Chem. Soc.* **2011**, *133*, 4250; d) B. C. Schroeder, Z. Huang, R. S. Ashraf, J. Smith, P. D'Angelo, S. E. Watkins, T. D. Anthopoulos, J. R. Durrant, I. McCulloch, *Adv. Funct. Mater.* **2012**, *22*, 1663; e) J. Hou, H.-Y. Chen, S. Zhang, G. Li, Y. Yang, *J. Am. Chem. Soc.* **2008**, *130*, 16144; f) R. C. Coffin, J. Peet, J. Rogers, G. C. Bazan, *Nat. Chem.* **2009**, *1*, 657.

[5] a) T. Baumgartner, R. Réau, *Chem. Rev.* **2006**, *106*, 4681; Correction **2007**, *107*, 303; b) J. Crassous, R. Réau, *Dalton Trans.* **2008**, 6865; c) Y. Matano, H. Imahori, *Org. Biomol. Chem.* **2009**, *7*, 1258; d) Y. Ren, T. Baumgartner, *Dalton Trans.* **2012**, *41*, 7792.

[6] a) D. J. Abdallah, A. Robertson, H.-F. Hsu, R. G. Weiss, *J. Am. Chem. Soc.* **2000**, *122*, 3053; b) H. Chen, D. C. Kwait, Z. S. Gönen, B. T. Weslowski, D. J. Abdallah, R. G. Weiss, *Chem. Mater.* **2002**, *14*, 4063; c) G. A. Nagana Gowda, H. Chen, C. L. Khetrapal, R. G. Weiss, *Chem. Mater.* **2004**, *16*, 2101; d) K. Ma, A. A. Shahkhatuni, B. S. Somashekhar, G. A. N. Gowda, Y. Tong, C. L. Khetrapal, R. G. Weiss, *Langmuir* **2008**, *24*, 9843; e) K. Ma, B. S. Somashekhar, G. A. Nagana Gowda, C. L. Khetrapal, R. G. Weiss, *Langmuir* **2008**, *24*, 2746; f) K. Ma, K.-M. Lee, L. Minkova, R. G. Weiss, *J. Org. Chem.* **2009**, *74*, 2088; g) T. Ichikawa, M. Yoshio, A. Hamasaki, S. Taguchi, F. Liu, X.-b. Zeng, G. Ungar, H. Ohno, T. Kato, *J. Am. Chem. Soc.* **2012**, *134*, 2634.

[7] a) Y. Ren, W. H. Kan, M. A. Henderson, P. G. Bomben, C. P. Berlinguette, V. Thangadurai, T. Baumgartner, *J. Am. Chem. Soc.* **2011**, *133*, 17014; b) Y. Ren, W. H. Kan, V. Thangadurai, T. Baumgartner, *Angew. Chem.* **2012**, *124*, 4031; *Angew. Chem. Int. Ed.* **2012**, *51*, 3964; c) Y. Ren, T. Baumgartner, *Inorg. Chem.* **2012**, *51*, 2669; d) Y. Ren, F. Biegger, T. Baumgartner, *J. Phys. Chem. C* **2013**, *117*, 4748; e) X. M. He, J. B. Lin, W. H. Kan, T. Baumgartner, *Angew. Chem.* **2013**, DOI: 10.1002/ange.201303729; *Angew. Chem. Int. Ed.* **2013**, DOI: 10.1002/anie.201303729.

[8] a) U. H. F. Bunz, *Chem. Rev.* **2000**, *100*, 1605; b) J. M. Tour, *Acc. Chem. Res.* **2000**, *33*, 791; c) V. W.-W. Yam, *Acc. Chem. Res.* **2002**, *35*, 555.

[9] M. Meldal, C. W. Tornoe, *Chem. Rev.* **2008**, *108*, 2952.

[10] a) Y. Matano, M. Nakashima, H. Imahori, *Angew. Chem.* **2009**, *121*, 4062; *Angew. Chem. Int. Ed.* **2009**, *48*, 4002; b) Y. Matano, M. Nakashima, A. Saito, H. Imahori, *Org. Lett.* **2009**, *11*, 3338.

[11] a) T. Baumgartner, T. Neumann, B. Wirges, *Angew. Chem.* **2004**, *116*, 6323; *Angew. Chem. Int. Ed.* **2004**, *43*, 6197; b) T. Baumgartner, W. Bergmans, T. Kárpáti, T. Neumann, M. Nieger, L. Nyulászi, *Chem. Eur. J.* **2005**, *11*, 4687; c) Y. Dienes, M. Eggenstein, T. Kárpáti, T. C. Sutherland, L. Nyulászi, T. Baumgartner, *Chem. Eur. J.* **2008**, *14*, 9878; d) Y. Ren, Y. Dienes, S. Hettel, M. Parvez, B. Hoge, T. Baumgartner, *Organometallics* **2009**, *28*, 734.

[12] a) A. I. Arkhypchuk, M.-P. Santoni, S. Ott, *Organometallics* **2012**, *31*, 1118; b) C. J. Chua, Y. Ren, T. Baumgartner, *Organometallics* **2012**, *31*, 2425.

[13] T. Baumgartner, M. Fiege, F. Pontzen, R. Arteaga-Müller, *Organometallics* **2006**, *25*, 5657.

[14] a) S. Durben, T. Baumgartner, *Angew. Chem.* **2011**, *123*, 8096; *Angew. Chem. Int. Ed.* **2011**, *50*, 7948; b) S. Durben, T. Baumgartner, *Inorg. Chem.* **2011**, *50*, 6823.

[15] a) J. E. Anthony, *Chem. Rev.* **2006**, *106*, 5028; b) J. E. Anthony, *Angew. Chem.* **2008**, *120*, 460–492; *Angew. Chem. Int. Ed.* **2008**, *47*, 452.

[16] a) V. K. Praveen, S. J. George, R. Varghese, C. Vijayakumar, A. Ajayaghosh, *J. Am. Chem. Soc.* **2006**, *128*, 7542; b) C. Vijayakumar, V. K. Praveen, A. Ajayaghosh, *Adv. Mater.* **2009**, *21*, 2059.

[17] A similar FRET process was also observed with **3b** in the solid state, however to a lesser extent (Figure S12). By contrast, due to the insolubility of Rhodamine B in hexane, even in the presence of **3b-O**, the energy transfer from **3b-O** to Rhodamine B could not be achieved in the gel phase.

[18] a) E. J. Fernández, J. M. López-de-Luzuriaga, M. Monge, M. E. Olmos, J. Pérez, A. Laguna, A. A. Mohamed, J. P. Fackler, *J. Am. Chem. Soc.* **2003**, *125*, 2022; b) A. Laguna, T. Lasanta, J. M. López-de-Luzuriaga, M. Monge, P. Naumov, M. E. Olmos, *J. Am. Chem. Soc.* **2009**, *132*, 456; c) C. E. Strasser, V. J. Catalano, *J. Am. Chem. Soc.* **2010**, *132*, 10009; d) I. O. Koshevoy, Y.-C. Chang, A. J. Karttunen, M. Haukka, T. Pakkanen, P.-T. Chou, *J. Am. Chem. Soc.* **2012**, *134*, 6564.